

The Dual-microfacet Model for Capturing Thin Transparent Slabs

Qiang Dai^{1,2†} Jiaping Wang² Yiming Liu^{2,3†} John Snyder⁴ Enhua Wu^{1,5} Baining Guo²

¹Institute of Software, Chinese Academy of Sciences

²Microsoft Research Asia

³Nanyang Technological University

⁴Microsoft Research

⁵University of Macau

Abstract

We present a new model, called the dual-microfacet, for those materials such as paper and plastic formed by a thin, transparent slab lying between two surfaces of spatially varying roughness. Light transmission through the slab is represented by a microfacet-based BTDF which tabulates the microfacet's normal distribution (NDF) as a function of surface location. Though the material is bounded by two surfaces of different roughness, we approximate light transmission through it by a virtual slab determined by a single spatially-varying NDF. This enables efficient capturing of spatially variant transparent slices. We describe a device for measuring this model over a flat sample by shining light from a CRT behind it and capturing a sequence of images from a single view. Our method captures both angular and spatial variation in the BTDF and provides a good match to measured materials.

Categories and Subject Descriptors (according to ACM CCS): I.3.7 [Computer Graphics]: Three-Dimensional Graphics and Realism—Color, shading, shadowing, and texture

1. Introduction

Many common objects are thin-layer transparent slices bounded by rough surfaces, such as plastic or resin slices, textured, scratched, or stained glass, and cellulose sheets such as paper, film and dried leaves. Refractions at the rough surface interfaces cause complex shading effects such as spatially-varying light scattering, background blurring, and anisotropy. Capturing these reflectance properties improves realism but has proven a challenging problem.

Light transmission through a transparent material can be represented by a four-dimensional Bidirectional Transmission Distribution Function (BTDF) $\rho(\mathbf{i}, \mathbf{o})$, describing how much light is transmitted when lit from direction \mathbf{i} and viewed from direction \mathbf{o} . Unlike the BRDF, \mathbf{o} in the BTDF

always points to the hemisphere opposite \mathbf{i} , representing the direction of transmitted rather than reflected light.

Based on microfacet theory [CT82], several parametric BTDF models have been developed [Sta01, WMLT07]. Most previous works account only for a single rough surface whereas two refractive interfaces lie between light source and observer in the case of a thin transparent slab. We assume these two interfaces form two independent, rough surfaces and derive an approximation for light transmission through the pair, called the *dual-microfacet* model. Though each surface can be represented by a separate, spatially-varying normal distribution function, we form a virtual surface which provides identical light paths (assuming an infinitely thin slab) and which is determined by a single NDF. This is critical for developing efficient and robust methods for acquiring the model from real materials.

Accounting for spatial variation in light transmission then yields the six-dimensional Spatially Varying Bidirectional Transmission Distribution Function (SVBTDF) $\rho(\mathbf{x}, \mathbf{i}, \mathbf{o})$.

[†] This work was done when Qiang Dai and Yiming Liu were visiting students at Microsoft Research Asia.

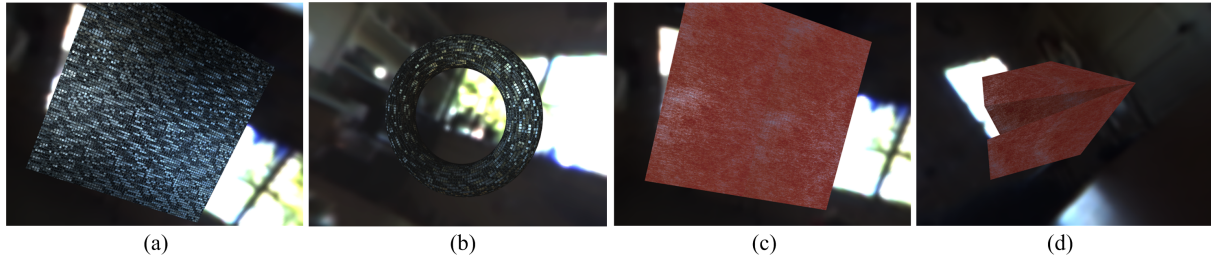


Figure 1: SVBTDFs acquired with our method from real world material samples having spatially varying, rough surfaces.

As with an SVBRDF, a straightforward way of measuring the SVBTDF adapts the gonioreflectometer [DNvGK99] by placing lamps behind the material sample. Densely scanning over light and view directions requires lengthy capture on expensive devices. Another approach represents the BTDF using a simple parametric model whose few parameters can be estimated from a sparse set or even a single image [GRBN07]. This reduces the acquisition workload, but fails to capture the richness of real-world BTDFs, especially anisotropy.

Using our dual-microfacet model, we present a new technique for measuring SVBTDFs from images of a surface sample taken from multiple light directions and a single view. A camera-monitor system acquires back-illuminated images of the material sample. Displaying a single dot on the monitor at different locations provides a controllable light direction and yields a 2D BTDF slice at each surface point. Instead of fitting a parameterized BTDF model to the captured data [WMLT07, GRBN07], we reconstruct an NDF from these BTDF slices and finally derive the dual-microfacet model.

Our major contribution is a new model (dual-microfacet) for thin transparent slabs. It describes the pair of refraction events at the slab boundaries by a single, local formula. This avoids costly integration of the two events in rendering (Equation 1) and difficult separation of the two events in acquisition. Ours is the first method for efficiently modeling and acquiring SVBTDFs including anisotropy.

2. Related Work

Microfacet Models for describing reflectance off rough surfaces were introduced to computer graphics by [CT82]. A number of parametric BRDF models based on this theory have been proposed [War92, LFTG97, AS00], which represent the distribution of microfacet normals (NDF) empirically using an analytic expression such as a Gaussian. These models are simple to evaluate and easy to acquire but roughly approximate the underlying microstructure and miss details in many real-world materials [NDM05]. [IA00] and [WW07] extend the microfacet model to mul-

iple layer surfaces. More general representations have thus been proposed to represent the NDF with a tabulated function [PF90, WAT92, APS00]. Microfacet models have also been applied to transparent materials to model their BTDF [Sta01, WMLT07]. In [WMLT07], a microfacet-based model called GGX was proposed to describe light transmission through a rough surface between media having a different refractive index. A 1D parametric model describes the NDF with respect to polar angle and can not be applied to anisotropic materials.

Thin Translucent Slabs were first investigated in [HK93]. Their model is dominated by light scattering inside the object and requires Monte Carlo simulation to evaluate. Simplified models have since been proposed based on a semi-analytic representation [Sta01] and limited to multiple scattering in thin-layer materials [DJ05, JMLH01]. Recently a model for a contamination layer on smooth transparent surfaces was proposed in [GRBN07]. Their results are visually similar to our model limited to isotropic transparent slabs.

Our model ignores light scattering inside the object and only considers scattering due to refraction events on the bounding surfaces. In capturing of real materials, we separate the multiple scattering component during preprocessing.

Acquisition of Spatially Varying Models from real materials can be straightforwardly done by acquiring 6D data [DNvGK99] using a gonioreflectometer. [GTHD03] proposed a simple device for acquiring a spatially varying Ward model [War92]. For BTDF models, previous work considers a single refraction interface only [Sta01, WMLT07]. Using such models to capture thin-layer materials is hard because the refracted light at the first interface is inside the object and can not be measured before it is modified by the next refraction. [WMLT07] proposed a smart method to solve this problem by gluing a hemisphere to the transparent material with an ideally smooth surface on its dome and a rough surface to be measured on the planar base of the dome. While the directional light comes from the dome side, refracted light exits the hemisphere perpendicularly effectively neglecting the influence of the second refraction. [GRBN07] proposed

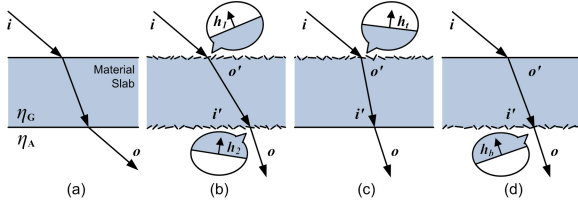


Figure 2: Dual-microfacet model. (a) Refraction through flat slab. (b) Refraction through rough slab. (c),(d) Equivalent refraction events are produced by a virtual configuration with a rough surface on one side and a flat surface on the other. The arrows show the directions of light transmission rather than the incoming or outgoing directions.

a device setup with a laser to measure the phase function at a particular point on a sample. Both works can only measure a single surface point at a time, and can only be inefficiently extended to measure spatial variation by scanning.

Our BTDF model combines the two refraction events together in a single, local formula which enables efficient acquisition of spatially varying materials. We reconstruct our model using data from a simple device that captures from a single view direction.

3. Dual-Microfacet Model

Microfacet theory represents surface microstructure with a large number of tiny mirror facets, each purely reflective and having the same refraction index, only with different orientations. The normal distribution function (NDF) $D(\mathbf{h})$ describes the distribution of microfacet orientations on the surface. It satisfies $D(\mathbf{h}) \geq 0$ and $\int_{\Omega_+} (\mathbf{n} \cdot \mathbf{h}) D(\mathbf{h}) d\omega_h = 1$ while the integration is done in half-angle space over the hemisphere

$$\Omega_+ = \Omega_+(\mathbf{n}) = \left\{ \mathbf{h} \mid \mathbf{h} \cdot \mathbf{n} > 0 \right\}.$$

where \mathbf{h} is the normal of microfacet, and \mathbf{n} is the surface normal.

Light traveling through a transparent slab refracts twice as it enters and exits. When the slab's bounding surfaces are ideally flat, light exits with the same direction it had originally as shown in Figure 2(a). The direction changes if the slab is bounded by a rough surface on both sides as shown in Figure 2(b). In this case, each refraction on the pair of boundary surfaces can be considered separately using previous models [Sta01, WMLT07] but this greatly complicates both rendering and acquisition.

To solve this problem, the first step in our model is to ignore the offset between the two refraction locations (i.e., assume an infinitely thin slab). The overall BTDF ρ is then roughly a convolution of the top and bottom BTDFs, ρ_t and

ρ_b . More precisely, it is given by

$$\rho(\mathbf{i}, \mathbf{o}) = \int_{\Omega_+} \rho_t(\mathbf{i}, \mathbf{w}) \rho_b(-\mathbf{w}, \mathbf{o}) d\omega_w. \quad (1)$$

Even with this approximation, (1) has no closed-form reduction in general and thus still entails costly numerical integration to evaluate during rendering. For acquisition, it is hard to separate the measured data in order to fit ρ_t and ρ_b .

We solve this problem by using microfacet theory to model the rough surfaces and combine the two refraction events. Surface microstructure is modeled with many tiny transparent facets, each purely refractive and having the same refractive index [CT82]. For a thin transparent slab bounded by rough surfaces as shown in Figure 2(b), the direction of transmitted light is given by Snell's law:

$$\mathbf{h}_1 = -\frac{\eta_A \mathbf{i} + \eta_G \mathbf{o}'}{\|\eta_A \mathbf{i} + \eta_G \mathbf{o}'\|}, \quad \mathbf{h}_2 = \frac{\eta_G \mathbf{i}' + \eta_A \mathbf{o}}{\|\eta_G \mathbf{i}' + \eta_A \mathbf{o}\|}. \quad (2)$$

where \mathbf{h}_1 and \mathbf{h}_2 are the microfacet normal directions of the first and second refraction, respectively. η_A and η_G are the refractive index of air and the transparent material, respectively. (2) assumes $\eta_G > \eta_A$. Substituting $\mathbf{i}' = -\mathbf{o}'$ into (2) yields the constraint

$$\mathbf{i} + \mathbf{o} = -\|\mathbf{i} + \eta \mathbf{o}'\| \mathbf{h}_1 + \|\mathbf{o} - \eta \mathbf{o}'\| \mathbf{h}_2 \quad (3)$$

where $\eta = \eta_G / \eta_A$ is the relative refractive index.

Consider the virtual configuration shown in Figure 2(c) which defines a rough surface on the top side of the slab in such a way as to yield an outgoing light direction which is the same as in (b). To find the microfacet normal direction \mathbf{h}_t of this virtual configuration, we plug $\mathbf{h}_2 = \mathbf{z}_+ = (0, 0, 1)$ into (3) to yield

$$\mathbf{h}_t = -\frac{\mathbf{i} + \mathbf{o} - \|\mathbf{o} - \mathbf{o}_m\| \mathbf{z}_+}{\|\mathbf{i} + \mathbf{o}_m\|} \quad (4)$$

where $\mathbf{o}_m = \eta \mathbf{o}' = (x_o, y_o, -\sqrt{\eta^2 - x_o^2 - y_o^2})$. The corresponding Jacobian multiplies the Jacobian of the two refraction events:

$$\left\| \frac{\partial \omega_{\mathbf{h}_t}}{\partial \omega_{\mathbf{o}}} \right\| = \left\| \frac{\partial \omega_{\mathbf{h}_t}}{\partial \omega_{\mathbf{o}'}} \right\| \left\| \frac{\partial \omega_{\mathbf{o}'}}{\partial \omega_{\mathbf{o}}} \right\| = \frac{|\mathbf{o} \cdot \mathbf{o}_m| |\mathbf{o}_m \cdot \mathbf{h}_t|}{\eta^2 (\mathbf{i} \cdot \mathbf{h}_t + \mathbf{o}_m \cdot \mathbf{h}_t)^2}. \quad (5)$$

Assuming no light is absorbed within the material slab, the resulting BTDF is given by

$$\tilde{\rho}_t(\mathbf{i}, \mathbf{o}) = \left\| \frac{\partial \omega_{\mathbf{h}_t}}{\partial \omega_{\mathbf{o}}} \right\| \frac{|\mathbf{i} \cdot \mathbf{h}_t| F(\mathbf{i} \cdot \mathbf{h}_t) F(\mathbf{i}' \cdot \mathbf{z}_+) G(\mathbf{i}, \mathbf{o}, \mathbf{h}_t) D(\mathbf{h}_t)}{|\mathbf{i} \cdot \mathbf{z}_+| |\mathbf{o} \cdot \mathbf{z}_+|} \quad (6)$$

where F is the Fresnel transmittance and G is the shadowing term. The function D is the normal distribution function that is recovered and tabulated in our method. For more details about the calculation of the Jacobian terms, please refer to Appendix.

Similar formulas can be derived for the other case in which the top side is ideally flat and the bottom is rough

as shown in Figure 2(d):

$$\mathbf{h}_b = \frac{\mathbf{i} + \mathbf{o} + \|\mathbf{i} - \mathbf{i}_m\| \mathbf{z}_+}{\|\mathbf{o} + \mathbf{i}_m\|} \quad (7)$$

$$\mathbf{i}_m = \eta \mathbf{i}' = \left(\mathbf{i}_x, \mathbf{i}_y, \sqrt{\eta^2 - \mathbf{i}_x^2 - \mathbf{i}_y^2} \right) \quad (8)$$

$$\left\| \frac{\partial \omega_{\mathbf{h}_b}}{\partial \omega_{\mathbf{o}}} \right\| = \frac{|\mathbf{o} \cdot \mathbf{h}_b|}{(\mathbf{i}_m \cdot \mathbf{h}_b + \mathbf{o} \cdot \mathbf{h}_b)^2} \quad (9)$$

$$\tilde{\rho}_b(\mathbf{i}, \mathbf{o}) = \left\| \frac{\partial \omega_{\mathbf{h}_b}}{\partial \omega_{\mathbf{o}}} \right\| \frac{|\mathbf{i}' \cdot \mathbf{h}_b| F(\mathbf{i}' \cdot \mathbf{h}_b) F(\mathbf{i} \cdot \mathbf{z}_+) G(\mathbf{i}, \mathbf{o}, \mathbf{h}_b) D(\mathbf{h}_b)}{|\mathbf{i}' \cdot \mathbf{z}_+| |\mathbf{o} \cdot \mathbf{z}_+|} \quad (10)$$

Though real objects exhibit roughness at both boundaries, these two configurations represent two extreme cases of a single rough surface. Both virtual configurations produce similar transmitted light because they are derived to reproduce the same light paths. However, (6) and (10) are different and the two models predict different light scattering behavior. This difference stems from the basic asymmetry that light entering a medium of higher index of refraction is biased toward the ‘‘South Pole’’ axis, while light leaving is biased away.

Figure 3 shows that our model matches the ground truth Monte Carlo result quite well in the two extreme cases, (a) and (b). It is less accurate in an intermediate case (c) where the ground truth lobe lies between the locations predicted by our two extreme models. We therefore propose our final BTDF model as the linear interpolation in logarithm space between these two virtual configurations:

$$\ln \tilde{\rho}(\mathbf{i}, \mathbf{o}) = \alpha \ln \tilde{\rho}_t(\mathbf{i}, \mathbf{o}) + (1 - \alpha) \ln \tilde{\rho}_b(\mathbf{i}, \mathbf{o}). \quad (11)$$

The weighting factor α indicates the relative roughness of the two surfaces (larger α indicates a rougher top surface). In our model, a single NDF is used to describe the overall effect to the combined refraction events on both sides. In our

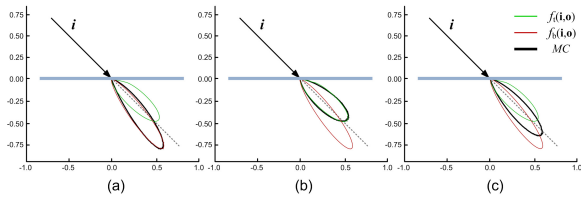


Figure 3: Comparing the virtual configuration with Monte Carlo photon tracing. (a) Only rough surface on the top. (b) Only rough surface on the bottom. (c) Both surfaces have the same level of roughness. The same Gaussian distribution of the microfacet orientation is used for the Monte Carlo photon tracing and the NDF $D(\mathbf{h})$ in our model. Refraction lobes predicted by the two models are compared to the ground truth shown by the gray dashed line.

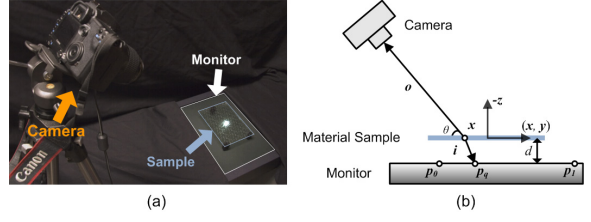


Figure 4: Our data acquisition device: (a) photograph, (b) diagram.

experiments, log space interpolation produces a better result than simple linear interpolation because the transmission effect at the two interfaces is essentially multiplicative.

Figure 5 compares this model with a single-refraction model (GGX) [WMLT07], based on Monte Carlo photon tracing ground truth. Our model predicts the refraction lobe more accurately.

4. Measuring Thin Transparent Slabs

To acquire the dual-microfacet model from a real-world material sample, a camera-monitor device is used to capture 2D BTDF slices at each surface point. Measured 2D BTDF slices are then interpolated to a regularly-sampled hemispherical function, and the dual-microfacet model is fitted at each surface point.

4.1. Refraction Data Acquisition

Data is acquired by illuminating the material sample from the back and capturing its transmitted image from one view. We display a white dot on a black background on the computer monitor (Dell Flatten Screen CRT Display) at different screen positions to produce a point light source at different locations p_q as shown in Figure 4(b). A 40×40 grid of dot positions is scanned, one at a time, yielding a sequence of

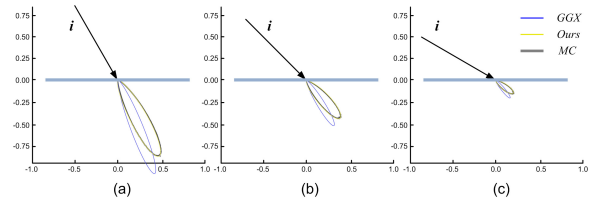


Figure 5: Comparison of our model vs. single-refraction. The same (Gaussian) distribution is used for the NDF in our model, GGX, Monte Carlo photon tracing. The testing material has the same level of surface roughness on both sides. The direction of the incoming light in (a), (b) and (c) is 30° , 45° and 60° , respectively. Our model with $\alpha = 0.56$ matches the Monte Carlo result better than GGX.

images I_q for $q \in S$ where S represents the set of dot locations. A Canon 30D camera with EF-100 2.8 lens is placed about 1.0m away and 0.7m above the center of the surface sample, making an angle of roughly $\theta = 45^\circ$ from vertical. The image resolution is 3504×2336 . We use a CRT display instead of an LCD because its radiance is more uniform with changing viewing angle.

Before capturing, we calibrate the camera's position and orientation as in [Zha00]. The color and intensity of the monitor is measured by directly capturing its output. We assume the CRT produces light that is uniform, both angularly and spatially.

Dots are displayed over a physical distance ranging from p_0 to p_1 as shown in Figure 4(b). This range is roughly 20% larger than the region of the material sample to be captured and is shifted in the direction opposite the camera by $d \cos \theta$, where d is the distance from the material sample to the monitor. In our experiments, we use $d = 0.04m$ and a square material size roughly $0.08m$ on each side. This yields a range of light directions producing an average 90° angular span around the ideal refraction direction. Dot positions are determined by capturing an image without the material sample. The dots are displayed simultaneously, detected in the image, and then projected to the 3D plane (x, y, d) .

After capturing, HDR images are reconstructed and rectified. The refraction function at each surface point \mathbf{x} can then be computed from the image sequence I_q , as

$$R(\mathbf{x}, \mathbf{i}_q(\mathbf{x}), \mathbf{o}) = \frac{I_q(\mathbf{x})}{(\mathbf{z}_+ \cdot \mathbf{i}_q(\mathbf{x}) L_q) \|p_q - \mathbf{x}\|^2} \quad (12)$$

where $I_q(x)$ is the color of the pixel at \mathbf{x} , p_q is the position of the light source in image q and L_q is its intensity. The lighting direction \mathbf{i} is computed as $\mathbf{i}_q(\mathbf{x}) = (p_q - \mathbf{x}) / \|p_q - \mathbf{x}\|$. Since the camera is quite far away from the sample, we use the same view direction $\mathbf{o}_c = V / \|V\|$ for all surface points, where V is the calibrated camera position.

In real materials, the transmission function includes (diffuse) multiple scattering effects as well as spatially-varying refraction. We model it via

$$R(\mathbf{x}, \mathbf{i}, \mathbf{o}) = \rho_d + k_s \rho(\mathbf{x}, \mathbf{i}, \mathbf{o}). \quad (13)$$

We then separate the diffuse from specular components using

$$\rho_d = \min_q \{R(\mathbf{x}, \mathbf{i}_q(\mathbf{x}), \mathbf{o}) | I_q(\mathbf{x}) > 0.05 I_{avg}\}. \quad (14)$$

according to the simple threshold technique in [WZT*08]. After separation, measurements of the refractive component $\rho(\mathbf{x}, \mathbf{i}, \mathbf{o})$ are irregularly scattered as a function of \mathbf{i} because of spatial variation in the lighting direction, $\mathbf{i}_q(\mathbf{x})$. We resample them onto a hemicube using the push-pull method [GGSC96], as in [WZT*08].

4.2. Model Fitting

We drop the position parameter \mathbf{x} in this subsection since each point is processed independently and equivalently. After the BTDF slice is recovered, we fit the dual-microfacet model to the measured data at each point by minimizing the difference between the refraction measured and prediction of our model. We assume the shadowing term $G(\mathbf{i}, \mathbf{o}, \mathbf{h})$ and the refractive index η are known. The unknown terms are thus the weighting factor α and the NDF $D(\mathbf{h})$. We propose an iterative method for model fitting which performs two steps in each iteration. The first estimates the NDF $D(\mathbf{h})$ while fixing the weight α , while the second searches for the best α while holding the NDF $D(\mathbf{h})$ constant.

More precisely, the NDF $D(\mathbf{h})$ is estimated in the first step by minimizing:

$$\min_D \sum_{q \in S} \|\ln \rho(\mathbf{i}_q, \mathbf{o}_c) - \ln \tilde{\rho}(\mathbf{i}_q, \mathbf{o}_c)\|^2 \quad (15)$$

For each measurement $\langle \mathbf{i}_q, \mathbf{o}_c \rangle$, $\tilde{\rho}$ is defined in (11) in terms of two normal directions \mathbf{h}_t and \mathbf{h}_b which define BTDFs according to (6) and (10). Because two directions are involved, we solve for the optimal D using a set of linear equations rather than the simple diagonal system of [NDM05, WZT*08]. The linear system is given by

$$\alpha \tilde{D}_{\mathbf{h}_t} + (1 - \alpha) \tilde{D}_{\mathbf{h}_b} = \ln \rho(\mathbf{i}_q, \mathbf{o}_c) - A, \quad q \in S \quad (16)$$

$$4\tilde{D}_{\mathbf{h}} - \tilde{D}_{\mathbf{h}_1} - \tilde{D}_{\mathbf{h}_2} - \tilde{D}_{\mathbf{h}_3} - \tilde{D}_{\mathbf{h}_4} = 0, \quad \mathbf{h} \in \Omega_+ \quad (17)$$

where $A = \alpha \ln A_t + (1 - \alpha) \ln A_b$ and $\tilde{D}_{\mathbf{h}} = \ln D(\mathbf{h})$. A_t and A_b are the products of the remaining terms in (6) and (10), excluding the unknown $D(\mathbf{h})$. \mathbf{o}_c is the viewing direction which is fixed and determined by the camera position. S is the set of light direction dots sampled as described in Section 4.1. The number of equations generated in (16) is the number of measurements $|S|$ ("Lights" in Table 1). We represent the hemispherical function D using a hemicube [WZT*08].

Equation (17) is added to regularize smoothness on unknowns that may not be adequately constrained by (16) alone. $\tilde{D}_{\mathbf{h}_i}, i \in \{1, \dots, 4\}$ in (17) represents the four neighboring cells of \mathbf{h} in the hemicube. Boundary hemicube cells are removed from the set of unknowns and set to $\ln \epsilon$. We use $\epsilon = 1 \times 10^{-6}$ which assumes the NDF boundary is close to zero. The number of equations generated in (17) is the number of non-boundary cells in the hemicube.

After estimating the NDF, the next step searches for an optimal weight factor α by mean incident direction weighted by the BTDF:

$$\min_\alpha \left\| \frac{\int_{\Omega_+} \mathbf{i} \rho(\mathbf{i}, \mathbf{o}_c) d\omega_{\mathbf{i}}}{\int_{\Omega_+} \rho(\mathbf{i}, \mathbf{o}_c) d\omega_{\mathbf{i}}} - \frac{\int_{\Omega_+} \mathbf{i} \tilde{\rho}(\mathbf{i}, \mathbf{o}_c) d\omega_{\mathbf{i}}}{\int_{\Omega_+} \tilde{\rho}(\mathbf{i}, \mathbf{o}_c) d\omega_{\mathbf{i}}} \right\|^2. \quad (18)$$

The minimum is found by golden section search [PTVF92] within $[0, 1]$. We initialize at $\alpha = 0.5$ and stop iterating when

α changes little (< 0.01). In our experiments, the iteration converges in fewer than 10 steps.

During a first-pass set of iterations, we constrain D to have polar symmetry via

$$\tilde{D}_{\mathbf{h}} - \tilde{D}_{\mathbf{h}'} = 0, \quad \mathbf{h} \in \Omega_+ \quad (19)$$

where $\mathbf{h}' = (-x_{\mathbf{h}}, -y_{\mathbf{h}}, z_{\mathbf{h}})$ is the polar-mirrored version of \mathbf{h} . This constraint provides a better estimate of D before the iteration has formed a good estimate of α . After convergence, $D(\mathbf{h})$ is computed once more, in a second pass without (19).

As previously mentioned, we assume the shadowing term is known. It has only a subtle effect on appearance. Unlike the case of the BRDF, in which the shadowing term moves opposite to the Fresnel factor, in a BTDF the shadowing term behaves consistently with the Fresnel factor, which falls off sharply away from normal incidence. We use the Smith model [Smi67] for the shadowing term, as in [WMLT07], which is controlled by the shadowing roughness parameter α_b . Iteration is first performed assuming $\alpha_b = 0.2$, after which we search for a better α_b subject to (15) while keeping α and $D(\mathbf{h})$ constant using the Levenberg-Marquardt algorithm [PTVF92]. The refractive index η of common materials can be found in a chemistry handbook such as [LBB*08].

4.3. Acceleration

The bottleneck of model reconstruction is the model fitting step at each surface point (i.e., at each pixel in the acquired images). Many measured BTDF slices are similar, yielding redundant fitting computation. We cluster the BTDF slices $\rho(\mathbf{x}, \mathbf{i}, \mathbf{o}_c)$ to a smaller number of representatives using k -means clustering. Model fitting is performed only on these representatives, indexed by j . After their models $\langle \alpha, D \rangle_j$ are reconstructed, the models for each non-representative point $\langle \alpha, D \rangle_i$ is linearly interpolated from its nearby representatives N_i in the vector space of BTDF slices:

$$\langle \alpha, D \rangle_i = \sum_{j \in N_i} w_{ij} \langle \alpha, D \rangle_j \quad (20)$$

where w_{ij} are the interpolation weights. These are determined by finding the best linear combination of nearby BTDF slices:

$$\sum_{j \in N_i} w_{ij} \rho_j(\mathbf{i}, \mathbf{o}) = \rho_i(\mathbf{i}, \mathbf{o}) \quad (21)$$

$$\sum_{j \in N_i} w_{ij} = 1 \quad (22)$$

We follow the same rules to determine the neighborhood set N_i in the representatives as in [WZT*08]. In our experiments, we choose 1% of the surface points as representatives, which yields a speed up of roughly 100 times.

5. Experimental Results

We validated our model using various sheets of real-world transparent materials captured with our simple device. Table

Sample	Image Res	Lights	NDF Res	η
Grid Sheet	600×600	40×40	32×32	1.4
Leaf Glass	400×420	40×40	32×32	1.5
Rice Paper	600×600	20×20	32×32	1.55

Table 1: Parameters for various material samples.

1 lists data for these samples including spatial resolution, angular resolution of NDFs, and refractive index.

We implemented our accelerated model fitting algorithm on a PC with Intel Core™2 Quad 2.13GHz CPU and 4GB memory. Data capturing takes about 5-10 hours using multiple-exposure acquisition. The angular sampling density for lighting is manually chosen depending on the roughness of the sample surfaces. Image data processing (including calibration, HDR reconstruction, diffuse separation, and resampling) takes about 3-4 hours, and is dominated by disk I/O. Model fitting with clustering acceleration takes about one hour. We integrated our BTDF model into a ray tracer for rendering results, only refraction on the first surface is rendered.

Figure 1 shows the rendering result of mapping our SVBTDF model to more complex geometry and under environment lighting. The images show spatially varying and anisotropic light scattering. Subtle color changes due to refracted light in the red rice paper are captured as well. The images are rendered with front face only. The tiling resolution in (a) and (c) is 2×2 .

Figure 6 shows a comparison of our model with a real image. The captured material is “Grid Sheet”, a piece of plastic window coating having highly anisotropic micro-structures as shown in (h). A novel view is used to test our rendering result in (b) which matches the real appearance in (a). We also visualize the NDFs (c-g, bottom row) by orthographic projection for surface points marked in (h). The NDFs constructed are consistent with the ground truth measured by shooting a laser beam at the same points [GRBN07]. Slight blurring is due to low hemicycle resolution.

Figure 7 compares the blurring effect on a background image. The leaf glass with rough pattern is put in the front of the checker board. Our result (b) provides a good match to the ground truth in (a) and preserves the spatial variation of blurring and anisotropy. However our result does not match the ground truth exactly, it is mainly due to the resolution limitation of NDF representation and the trade-off between sampled angular range and capturing time. For such a highly anisotropy material, both the angular range and the density of the sampled lighting direction should be high, which would require much more time and storage for data acquisition and processing.

6. Conclusion

We have proposed a novel microfacet-based BTDF for modeling the entire enter-then-exit light path through thin transparent slabs. The model is based on an NDF and a parameter controlling the roughness ratio between the top and bottom slab surfaces. Our model is easy to evaluate for rendering and provides better accuracy compared to single refraction models. It also enables easy acquisition of spatially varying materials, which we demonstrate successfully on 3 real-world materials using data captured from a simple device.

Our approach is limited to thin, transparent slices. Thick slabs yield a significant, angularly-dependent offset where the refracted light strikes the second interface, making our model inappropriate. In this case, parallax effect will not be captured. For materials with very sharp specular lobes, dense sampling of lights is required to capture the specular peak. Translucent materials with significant internal scattering are simplified by a diffuse term and thus not captured accurately.

In future work, we are interested in handling the view-dependent shifting of refracted light for transparent slices of a specified thickness. Generalizing the microfacet model to capture single and multiple scattering inside translucent materials is another extension. Finally, it is valuable to explore efficient methods for rendering SVBTDF models.

Acknowledgement: We would like to thank the anonymous reviewers for their valuable comments and insightful suggestions. This work was supported by the National Basic Research Program of China (Grant No. 2009CB320802), the National High Technology Research and Development

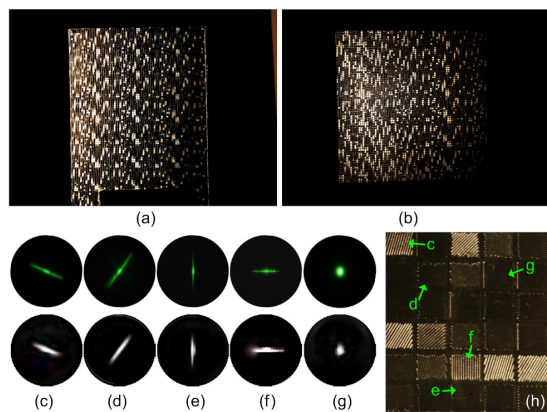


Figure 6: Model validation. (a) Real image. (b) Synthesized image using our model. The comparison uses a similar lighting direction; texture mapping in the synthesized image does not reproduce the global texture pattern. Columns (c-g) compare the NDFs (white, bottom) constructed with our method with the ground truth (green, top). The corresponding positions of these NDFs are marked in a close-up view of the captured material (h).

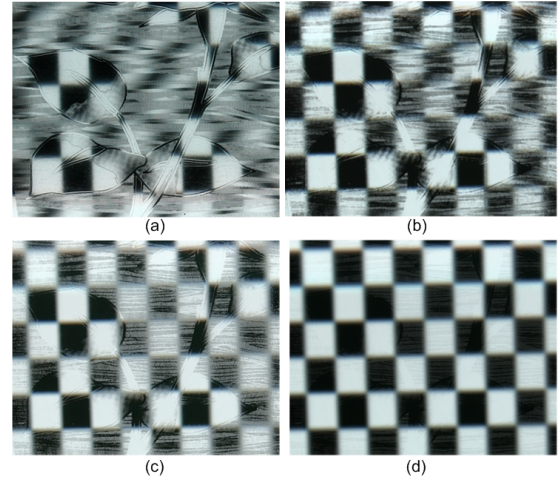


Figure 7: Blurring effect on background image. (a) Real image. (b) Our Method. (c) GGX Model [WMLT07]. (d) Dirty Glass Model [GRBN07]. Our result is closest to the real image. The GGX model yields isotropic blurring of the background image and an image shift due to incorrect prediction of refracted light directions in the dual interface. The Dirty Glass Model produces only uniform blurring of the background image.

Program of China (Grant No. 2008AA01Z301), and the Research Grant of the University of Macau.

References

- [APS00] ASHIKMIN M., PREMOŽE S., SHIRLEY P.: A microfacet-based BRDF generator. In *Proceedings of ACM SIGGRAPH 2000, Computer Graphics Proceeding, Annual Conference Series* (New York, NY, USA, 2000), ACM Press/Addison-Wesley Publishing Co., pp. 65–74.
- [AS00] ASHIKMIN M., SHIRLEY P.: An anisotropic phong BRDF model. *Journal of Graphics Tools* 5, 2 (2000), 25–32.
- [CT82] COOK R. L., TORRANCE K. E.: A reflectance model for computer graphics. *ACM Trans. Graph.* 1, 1 (1982), 7–24.
- [DJ05] DONNER C., JENSEN H. W.: Light diffusion in multi-layered translucent materials. In *SIGGRAPH '05: ACM SIGGRAPH 2005 Papers* (New York, NY, USA, 2005), ACM, pp. 1032–1039.
- [DNvGK99] DANA K. J., NAYAR S. K., VAN GINNEKEN B., KOENDERINK J. J.: Reflectance and texture of real-world surfaces. *ACM Transactions on Graphics* 18, 1 (1999), 1–34.
- [GGSC96] GORTLER S. J., GRZESZCZUK R., SZELISKI R., COHEN M. F.: The lumigraph. In *Proceedings of ACM SIGGRAPH 1996, Computer Graphics Proceeding, Annual Conference Series* (New York, NY, USA, 1996), ACM, pp. 43–54.
- [GRBN07] GU J., RAMAMOORTHY R., BELHUMEUR P., NAYAR S.: Dirty glass: Rendering contamination on transparent surfaces. *Eurographics Symposium on Rendering* (June 2007), 159–170.
- [GTHD03] GARDNER A., TCHOU C., HAWKINS T., DEBEVEC P.: Linear light source reflectometry. *ACM Transactions on Graphics* 22, 3 (2003), 749–758.

- [HK93] HANRAHAN P., KRUEGER W.: Reflection from layered surfaces due to subsurface scattering. In *SIGGRAPH '93: Proceedings of the 20th annual conference on Computer graphics and interactive techniques* (New York, NY, USA, 1993), ACM, pp. 165–174.
- [IA00] ICART I., ARQUÈS D.: A physically-based BRDF model for multilayer systems with uncorrelated rough boundaries. In *Proceedings of the Eurographics Workshop on Rendering Techniques 2000* (London, UK, 2000), Springer-Verlag, pp. 353–364.
- [JMLH01] JENSEN H. W., MARSCHNER S. R., LEVOY M., HANRAHAN P.: A practical model for subsurface light transport. In *SIGGRAPH '01: Proceedings of the 28th annual conference on Computer graphics and interactive techniques* (New York, NY, USA, 2001), ACM, pp. 511–518.
- [LBB*08] LIDE D. R., BAYSINGER G., BERGER L. I., GOLDBERG R. N., KEHIAIAN H. V., KUCHITSU K., ROSENBLATT G., ROTH D. L., ZWILLINGER D.: Handbook of chemistry and physics, 88th edition. *Chapman & Hall/CRC Press LLC* (2008).
- [LFTG97] LAFORTUNE E. P. F., FOO S.-C., TORRANCE K. E., GREENBERG D. P.: Non-linear approximation of reflectance functions. In *Proceedings of ACM SIGGRAPH 1997, Computer Graphics Proceeding, Annual Conference Series* (New York, NY, USA, 1997), ACM Press/Addison-Wesley Publishing Co., pp. 117–126.
- [NDM05] NGAN A., DURAND F., MATUSIK W.: Experimental analysis of BRDF models. In *Rendering Techniques 2005: 16th Eurographics Workshop on Rendering* (June 2005), pp. 117–126.
- [PF90] POULIN P., FOURNIER A.: A model for anisotropic reflection. In *Computer Graphics (Proceedings of ACM SIGGRAPH 90)* (Aug. 1990), Baskett F., (Ed.), vol. 24, pp. 273–282.
- [PTVF92] PRESS W. H., TEUKOLSKY S. A., VETTERLING W. T., FLANNERY B. P.: Numerical recipes in C (second edition). *Cambridge University Press* (1992).
- [Smi67] SMITH B. G.: Geometrical shadowing of a random rough surface. *IEEE Transactions on Antennas and Propagation*, 15 (1967), 668 – 671.
- [Sta01] STAM J.: An illumination model for a skin layer bounded by rough surfaces. In *Proceedings of the 12th Eurographics Workshop on Rendering Techniques* (London, UK, 2001), Springer-Verlag, pp. 39–52.
- [War92] WARD G. J.: Measuring and modeling anisotropic reflection. In *Computer Graphics (Proceedings of ACM SIGGRAPH 92)* (New York, NY, USA, 1992), ACM Press, pp. 265–272.
- [WAT92] WESTIN S. H., ARVO J. R., TORRANCE K. E.: Predicting reflectance functions from complex surfaces. In *Computer Graphics (Proceedings of ACM SIGGRAPH 92)* (New York, NY, USA, 1992), ACM Press, pp. 255–264.
- [WMLT07] WALTER B., MARSCHNER S. R., LI H., TORRANCE K. E.: Microfacet models for refraction through rough surfaces. *Eurographics Symposium on Rendering* (June 2007), 195–206.
- [WW07] WEIDLICH A., WILKIE A.: Arbitrarily layered microfacet surfaces. In *GRAPHITE 2007* (Dec. 2007), ACM, pp. 171–178.
- [WZT*08] WANG J., ZHAO S., TONG X., SYNDER J., GUO B.: Modeling anisotropic surface reflectance with example-based microfacet synthesis. *ACM Transactions on Graphics (SIGGRAPH 2008)* 27, 3 (August 2008), 41:1–41:9.
- [Zha00] ZHANG Z.: A flexible new technique for camera calibration. In *IEEE Transactions on Pattern Analysis and Machine Intelligence* (2000), vol. 22, pp. 1330–1334.

Appendix

Jacobian Calculation in Dual Refraction

Figures 2(c) and (d) show the two extreme configurations. The refractive index of the slab is η_G and the surrounding is η_A . We use the relative refractive index $\eta = \eta_G/\eta_A$ in all formulas.

Consider the virtual configuration shown in Figure 2(c) which defines a rough surface only on the top side of the slab. The microfacet normal direction \mathbf{h}_t is determined as (4), where $\mathbf{o}_m = \eta\mathbf{o}' = (x_o, y_o, -\sqrt{\eta^2 - x_o^2 - y_o^2})$. The corresponding Jacobian multiplies the Jacobian of the two refraction events:

$$\left\| \frac{\partial \omega_{\mathbf{h}_t}}{\partial \omega_{\mathbf{o}'}} \right\| = \left\| \frac{\partial \omega_{\mathbf{h}_t}}{\partial \omega_{\mathbf{o}_m}} \right\| \left\| \frac{\partial \omega_{\mathbf{o}_m}}{\partial \omega_{\mathbf{o}'}} \right\|. \quad (23)$$

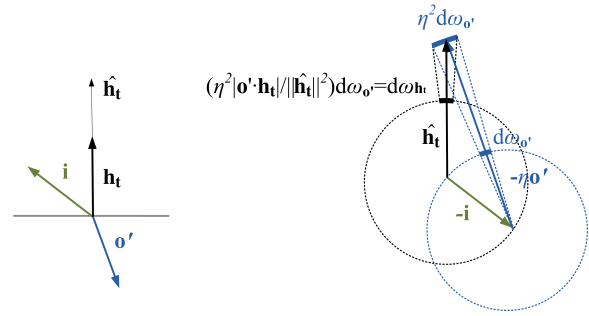


Figure 8: Geometry for first ideal refraction event in Figure 2(c), with half-vector $\hat{\mathbf{h}}_t = -\mathbf{i} - \eta\mathbf{o}'$ and normalized half-direction $\mathbf{h}_t = \hat{\mathbf{h}}_t / \|\hat{\mathbf{h}}_t\|$. We compute the Jacobian by taking an infinitesimal solid angle perturbation $d\omega_{\mathbf{o}'}$ in \mathbf{o}' , projecting into a perturbation in \mathbf{h}_t and then onto the unit sphere for \mathbf{h}_t . Only the 2D incidence plane slice through the full 3D space is shown.

The first Jacobian in (23) is derived exactly as the Equation 17 in [WMLT07], as shown in Figure 8:

$$\left\| \frac{\partial \omega_{\mathbf{h}_t}}{\partial \omega_{\mathbf{o}'}} \right\| = \frac{\eta^2 |\mathbf{o}' \cdot \mathbf{h}_t|}{(\mathbf{i} \cdot \mathbf{h}_t + \eta (\mathbf{o}' \cdot \mathbf{h}_t))^2} \quad (24)$$

Plug $\mathbf{o}_m = \eta\mathbf{o}'$ into (24), we have:

$$\left\| \frac{\partial \omega_{\mathbf{h}_t}}{\partial \omega_{\mathbf{o}'}} \right\| = \frac{\eta |\mathbf{o}_m \cdot \mathbf{h}_t|}{(\mathbf{i} \cdot \mathbf{h}_t + \mathbf{o}_m \cdot \mathbf{h}_t)^2} \quad (25)$$

A geometry explanation of calculating the second Jacobian in (23) is shown in Figure 9. The second Jacobian is finally derived as:

$$\left\| \frac{\partial \omega_{\mathbf{h}_t}}{\partial \omega_{\mathbf{o}'}} \right\| = \frac{|\mathbf{o} \cdot \mathbf{i}'|}{\eta^2} = \frac{|\mathbf{o} \cdot \mathbf{o}_m|}{\eta^3} \quad (26)$$

Finally we combined two Jacobian just as (5) in our paper.

Similar formulas can be derived for another extreme case which the top side is ideally flat and the bottom is rough as

shown in Figure 2(d). The microfacet normal direction \mathbf{h}_b is determined in (7), where $\mathbf{i}_m = \eta \mathbf{i}' = (\mathbf{i}_x, \mathbf{i}_y, \sqrt{\eta^2 - \mathbf{i}_x^2 - \mathbf{i}_y^2})$. In this case, the Jacobian is solely related to the second refraction event, as shown in Figure 10, the Jacobian is (9).

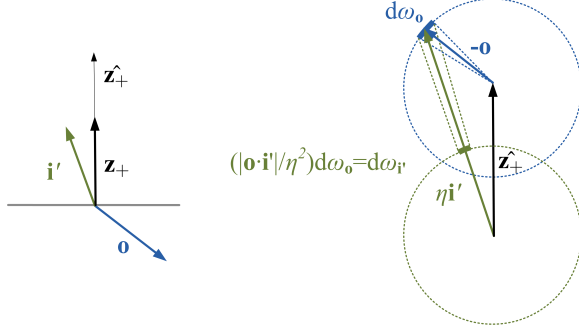


Figure 9: Geometry for the second ideal refraction event in Figure 2(c), with half-vector $\mathbf{z}_+ = \eta \mathbf{i}' + \mathbf{o}$ and normalized half-direction $\mathbf{z}_+ = \mathbf{z}_+ / \|\mathbf{z}_+\|$. We compute the Jacobian by taking an infinitesimal solid angle perturbation $d\omega_o$ in \mathbf{o} , projecting into a perturbation onto the unit sphere for \mathbf{i}' . Only the 2D incidence plane slice through the full 3D space is shown.

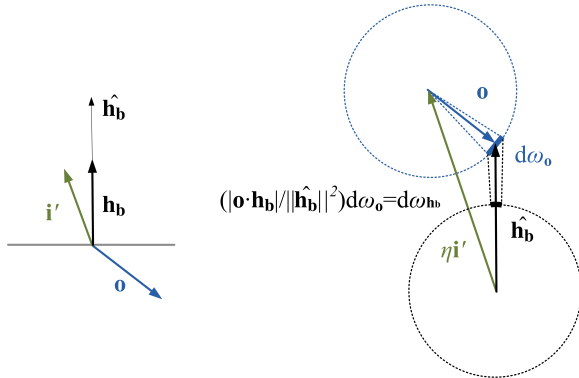


Figure 10: Geometry for second ideal refraction event in Figure 2(d), with half-vector $\hat{\mathbf{h}}_b = \eta \mathbf{i}' + \mathbf{o}$ and normalized half-direction $\mathbf{h}_b = \hat{\mathbf{h}}_b / \|\hat{\mathbf{h}}_b\|$. We compute the Jacobian by taking an infinitesimal solid angle perturbation $d\omega_o$ in \mathbf{o} , projecting into a perturbation onto the unit sphere for \mathbf{h}_b . Only the 2D incidence plane slice through the full 3D space is shown.